Inorganic Chemistry

Article

pubs.acs.org/IC

Drastic Effect of Lattice Propionitrile Molecules on the Spin-Transition Temperature of a 2,2′-Dipyridylamino/s-triazine-Based Iron(II) Complex

Nanthawat Wannarit,[†,‡,○] Nassim Nassirinia,[†,§] Saeid Amani,[§] Norberto Masciocchi,*[,∥] Sujittra Youngme,[‡] Olivier Roubeau,*[,⊥] Simon J. Teat,[#] and Patrick Gamez*[,†,▽]

[†]Departament de Química Inorgànica, Universitat de Barcelona, Martí i Franquès 1-11, 08028 Barcelona, Spain

[‡]Materials Chemistry Research Unit, Department of Chemistry and Center of Excellence for Innovation in Chemistry, Faculty of Science, Khon Kaen University, Khon Kaen 40002, Thailand

[§]Faculty of Sciences, Department of Chemistry, Arak University, Arak 38156-8-8349, Iran

[∥]Dipartimento di Scienza e Alta Tecnologia and To.Sca.Lab, Università dell'Insubria, Via Valleggio 11, 22100 Como, Italy

[⊥]Instituto de Ciencia de Materiales de Aragón (ICMA), CSIC and Universidad de Zaragoza, Plaza San Francisco s/n, 50009 Zaragoza, Spain

[#]Advanced Light Source (ALS), Lawrence Berkeley National Laboratory, 1 Cyclotron Road, Berkeley, California 94720, United States

[▽]Institució Catalana de Recerca i Estudis Avançats (ICREA), Passeig Lluís Companys 23, 08010 Barcelona, Spain

Supporting Information

ABSTRACT: Reaction of iron(II) selenocyanate (obtained from $Fe(ClO_4)_2$ and KNCSe) with 2-(*N*,*N*-bis(2-pyridyl)amino)-4,6-bis(pentafluorophenoxy)-(1,3,5)triazine (**L1**^{F}) in propionitrile produces the compound $[Fe(\mathbf{L1}^{F})_2(NCSe)_2]\cdot 2CH_3CH_2CN$ (**1**^{NCSe}**·2PrCN**), which shows spin-crossover (SCO) properties characterized by a $T_{1/2}$ of 283 K and a ΔT_{80} (i.e., temperature range within which 80% of the transition considered occurs) of about 65 K. Upon air exposure, **1**^{NCSe}**·2PrCN** gradually converts to a new SCO species that exhibits different properties, as reflected by $T_{1/2}$ = 220 K and ΔT_{80} = 70 K. Various characterization techniques, namely, IR spectroscopy, thermogravimetric analysis, and thermodiffractometric studies, reveal that the new phase is obtained through the loss of the lattice propionitrile molecules within several days upon air exposure or several hours upon heating above 390 K.

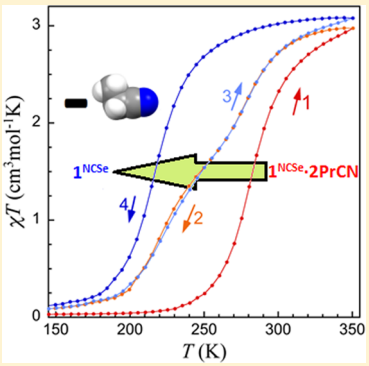

INTRODUCTION

The spin-crossover (SCO) phenomenon is a particular property of d^4−d^7 transition metal ions in which they may change their spin state from low spin (LS) to high spin (HS) and vice versa when appropriate donor atoms are coordinated to the metal centers, providing intermediate ligand-field strength.[1−3] This HS ↔ LS conversion may occur through the application of an external stimulus such as temperature, light, or pressure.[1,4−6]

SCO was first observed in 1931 by Cambi and co-workers, who serendipitously discovered that the magnetic properties of iron(III) coordination compounds of the type [Fe(dithiocarbamate)$_3$] showed temperature-dependent reversibility of their magnetic moments, from $\mu_{eff} \approx 1.9\mu_B$ ($S = {}^1/_2$) at low temperatures to $\mu_{eff} \approx 5.9\mu_B$ ($S = 5/2$) at higher ones.[7] More than eight decades later, SCO represents an important research area of molecular magnetism, as illustrated by the continuously growing number of groups worldwide that are devoted to the design and investigation of new SCO materials.[8] The great potential of SCO compounds toward practical applications was recognized with 1D coordination polymers of the type $\{Fe^{II}(4\text{-R-}1,2,4\text{-triazole})_3]X_2\}_n$ (for instance, with R = H or NH_2 and X = BF_4^- or NO_3^-), which show room-temperature spin transition associated with wide hysteresis loops.[9−12] Such materials have indeed been used to conceive a display device.[11,13] Thus, the switching properties of these "bistable" molecules make them highly attractive because they may find a number of applications in molecular electronics.[11,14−19]

Most iron-based SCO compounds are iron(II) complexes with a [FeN$_6$] octahedral geometry that is typically formed by aromatic nitrogen donor groups, e.g., pyridine or azole rings.[20−25] For about 7 years, we have been developing a family of ligands based on 2,2′-dipyridylamine (dpa) unit(s) attached to a 1,3,5-triazine (or *s*-triazine) ring.[26] The first member of this family, namely, 2,4,6-tris(dipyridin-2-ylamino)-1,3,5-triazine (dpyatriz), was reported by some of us in 2003.[27]

Received: June 17, 2014
Published: August 26, 2014

   dx.doi.org/10.1021/ic501389s | *Inorg. Chem.* 2014, 53, 9827−9836

This ligand, containing three dpa groups on the *s*-triazine ring,[28] allowed for the preparation of iron(II) coordination compounds with attracting SCO properties.[26,29,30] Concurrently, Murray and co-workers have described a number of dipyridylamino-substituted-triazine ligands, which have engendered various SCO materials exhibiting diverse transition properties.[31−36] Recently, we have described the iron(II) complex *trans*-$[Fe(\mathbf{L1^F})_2(NCS)_2]\cdot 2CH_3CN$ ($\mathbf{1^{NCS}\cdot 2MeCN}$), with $\mathbf{L1^F}$ = 2-(*N*,*N*-bis(2-pyridyl)amino)-4,6-bis(pentafluorophenoxy)-(1,3,5)triazine, which exhibits a relatively cooperative SCO character.[37] In the present study, we report on the preparation and characterization of the comparable selenocyanate analogue complex $[Fe(\mathbf{L1^F})_2(NCSe)_2]\cdot 2CH_3CH_2CN$ ($\mathbf{1^{NCSe}\cdot 2PrCN}$), which shows solvent-dependent SCO properties.[38−41] These particular features are unraveled through thermal, magnetic, and variable-temperature structural studies, which are analyzed and compared with the properties of related compounds.

RESULTS AND DISCUSSION

Synthesis and Crystal Structure of Compound $\mathbf{1^{NCSe}}$. The ligand 2-(*N*,*N*-bis(2-pyridyl)amino)-4,6-bis(pentafluorophenoxy)-(1,3,5)triazine ($\mathbf{L1^F}$) was prepared as described earlier for the preparation of $\mathbf{1^{NCS}\cdot 2MeCN}$.[37] Compound $\mathbf{1^{NCSe}\cdot 2PrCN}$, i.e., $[Fe(\mathbf{L1^F})_2(NCSe)_2]\cdot 2CH_3CH_2CN$, was obtained with a yield of 60% by reaction of iron(II) perchlorate hexahydrate (1 equiv), potassium selenocyanate (1 equiv), and ligand $\mathbf{L1^F}$ (2 equiv), as explained in the Experimental Section. $\mathbf{1^{NCSe}\cdot 2PrCN}$ is triclinic, space group $P\bar{1}$, in the whole 100−300 K range (single-crystal data collections performed at 100, 200, 260, and 300 K, Table S1). A representation of the molecular structure of $\mathbf{1^{NCSe}}$ at 100 K (low-spin state) is depicted in Figure 1. Selected bond lengths and angles are listed in Table 1.

The coordination environment of the iron(II) ion in $\mathbf{1^{NCSe}}$ is analogous to that of the previously reported compound $\mathbf{1^{NCS}}$.[37] The octahedral geometry is formed by two $\mathbf{L1^F}$ ligands in the equatorial plane and two *trans*, N-coordinated selenocyanate anions (Figure 1). The $Fe-N_{pyridine}$ bond lengths of 1.981(1) (Fe−N2) and 1.979(1) Å (Fe−N3) are representative of an LS iron(II) ion (Table 1). Consistently, the $Fe-N_{NCSe}$ distances of 1.930(1) Å are also indicative of an LS state. Actually, all Fe−N coordination distances observed in $\mathbf{1^{NCSe}}$ are very similar to those of the related thiocyanate compound $\mathbf{1^{NCS}}$ (measured at 100 K).[37] At 300 K, these bond lengths increase by ca. 0.17 Å ($Fe-N_{pyridine}$) and 0.11 Å ($Fe-N_{NCSe}$) (Table 1), hence illustrating the occurrence of a full (i.e., 100%) spin transition that is corroborated by variable-temperature magnetic susceptibility measurements (see Magnetic and Thermal Studies section). Such bond distance variations are typical for this type of SCO FeN_6 system.[42] Finally, the distances observed for $\mathbf{1^{NCSe}\cdot 2PrCN}$ at 260 K, i.e., 2.007(4)−2.011(3) Å for Fe−

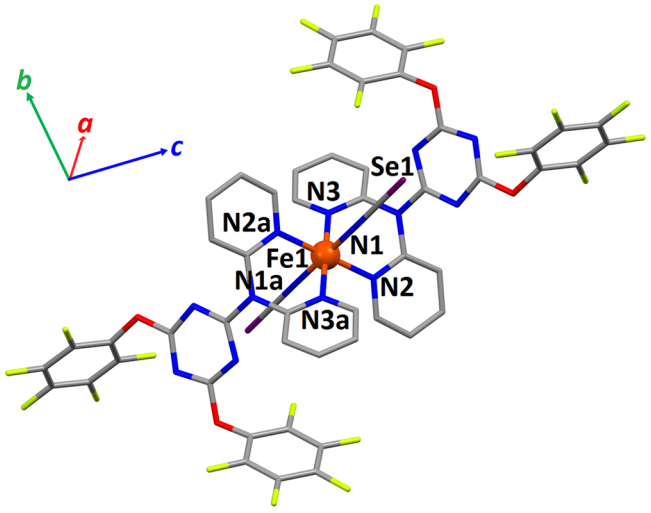

Figure 1. Representation of the molecular structure of the iron(II) complex $\mathbf{1^{NCSe}\cdot 2PrCN}$ (LS state, determined at 100 K) with partial atom-numbering scheme. Hydrogen atoms and lattice propionitrile molecules are not shown for clarity. Symmetry operation: $a = 1 - x, 1 - y, 1 - z$.

Table 1. Coordination Bond Lengths (Å) and Angles (Deg) and Supramolecular Interactions for Compound $\mathbf{1^{NCSe}}$·2PrCN at Three Different Temperatures[a]

bond	100 K (LS)	260 K	300 K (HS)
Fe1−N1	1.930(1)	1.948(3)	2.037(5)
Fe1−N2	1.981(1)	2.011(3)	2.161(3)
Fe1−N3	1.979(1)	2.007(4)	2.150(4)
$Fe1\cdots Fe1_{inter}$[b]	8.468(1)	8.638(3)	8.807(4)
angle	100 K (LS)	260 K	300 K (HS)
N2−Fe1−N3	86.25(6)	85.75(14)	82.85(13)
N3−Fe1−N2a	93.75(6)	94.25(14)	97.15(13)
N1−Fe1−N1a	180	180	180
ΣFe[c]	31	34	44
Φ[d]	25	40	64
$\pi\cdots\pi$ interactions[a]	100 K (LS)	260 K	300 K (HS)
O1···C19g	3.199(3)	3.205(6)	3.221(8)
O1···C20g	3.076(2)	3.119(6)	3.138(7)
C15···C20g	3.323(2)	3.350(6)	3.348(7)
Cg6···Cg6g	4.589(1)	4.603(3)	4.623(4)
C8···C10p	3.555(2)	3.589(6)	3.605(3)
C7···C10p	3.654(2)	3.736(5)	3.762(3)
C9···N3p	3.700(2)	3.783(6)	3.806(2)
Cg4···Cg4p	3.682(1)	3.764(3)	3.786(3)
halogen···halogen contacts[a]	100 K (LS)	260 K	300 K (HS)
F4···F7e	2.885(2)	2.933(5)	2.937(7)
F8···F9k	2.780(2)	2.852(5)	2.872(7)
lone pair···π interactions[a]	100 K (LS)	260 K	300 K (HS)
N7···F1c	3.104(2)	3.305(2)	3.268(7)
C12···F2c	3.014(2)	3.024(5)	3.047(7)
F1c···Cg5	3.238(2)	3.360(4)	3.478(5)
F2c···Cg5	3.443(2)	3.401(4)	3.398(5)
N1S···C21	3.202(3)	3.312(7)	3.332(10)
N1S···C26	3.278(3)	3.261(8)	3.320(11)
N1S···Cg7	3.413(2)	3.399(7)	3.466(10)
Se1···C22b	3.531(2)	3.663(5)	3.720(6)
Se1···C23b	3.772(2)	3.906(5)	3.935(5)
Se1···F6b	3.192(1)	3.239(3)	3.269(4)
Se1···Cg7	4.320(1)	4.486(3)	4.552(4)
Se1···C13	3.697(2)	3.755(4)	3.789(5)
Se1···Cg5	3.585(1)	3.654(2)	3.722(2)

[a]Symmetry operations: $a = 1 - x, 1 - y, 1 - z$; $b = -1 + x, y, z$; $c = 2 - x, 1 - y, 2 - z$; $e = 2 - x, 2 - y, 2 - z$; $g = 1 - x, 1 - y, 2 - z$; $k = 2 - x, 2 - y, 1 - z$; $p = 2 - x, 1 - y, 1 - z$. [b]Closest intermonomer Fe···Fe distance (observed along the crystallographic *a* axis). [c]$\sum$ = the sum of $|90 - \theta|$ for the 12 N−Fe−N angles in the octahedron.[65,66] [d]Φ = sum of $|60 - \theta|$ for the 24 N−Fe−N angles describing the trigonal twist angle.[43,44]

dx.doi.org/10.1021/ic501389s | Inorg. Chem. 2014, 53, 9827−9836

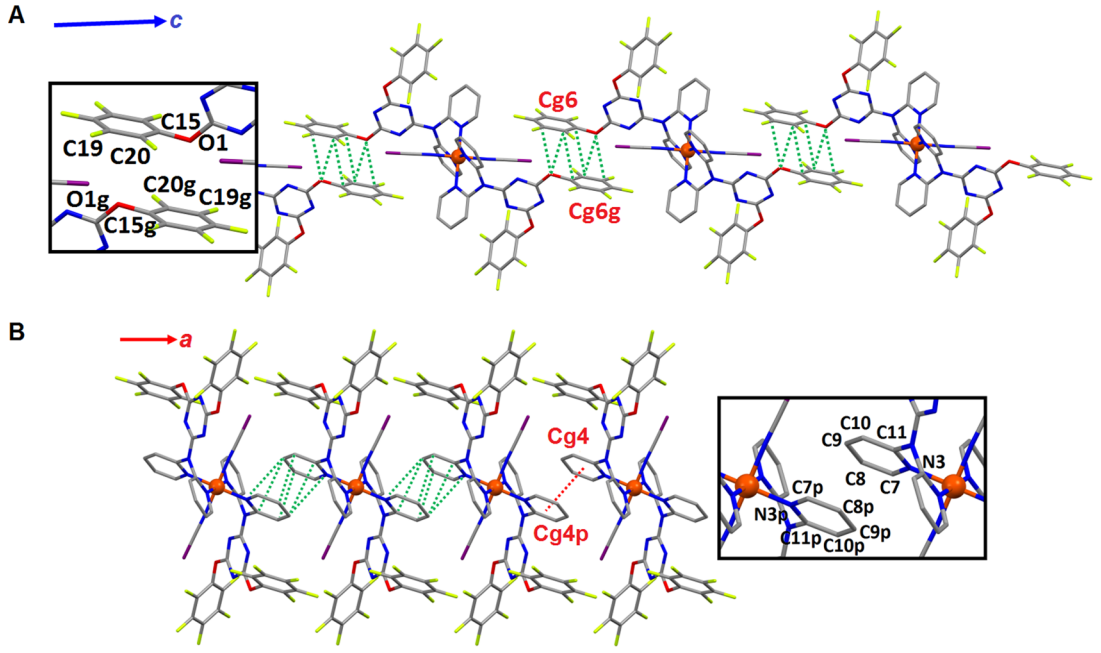

Figure 2. Views of the crystal packing of LS $\mathbf{1}^{NCSe}$**·2PrCN** showing (A) the formation of a supramolecular 1D chain along the crystallographic *c* axis by means of parallel-displaced $\pi\cdots\pi$ interactions between pentafluorophenoxy rings, with Cg6···Cg6g = 4.589(1) Å (the inset shows the labeling of the atoms involved in short supramolecular contacts (see Table 1), which are displayed as green dotted lines), and (B) the formation of a supramolecular 1D chain along the crystallographic *a* axis by means of $\pi\cdots\pi$ interactions between coordinated pyridine moieties, with Cg4···Cg4p = 3.682(1) Å (red dotted line) (the inset shows the labeling of the atoms involved in short supramolecular contacts (see Table 1), which are displayed as green dotted lines). Symmetry operations: $g = 1 - x, 1 - y, 2 - z$; $p = 2 - x, 1 - y, 1 - z$.

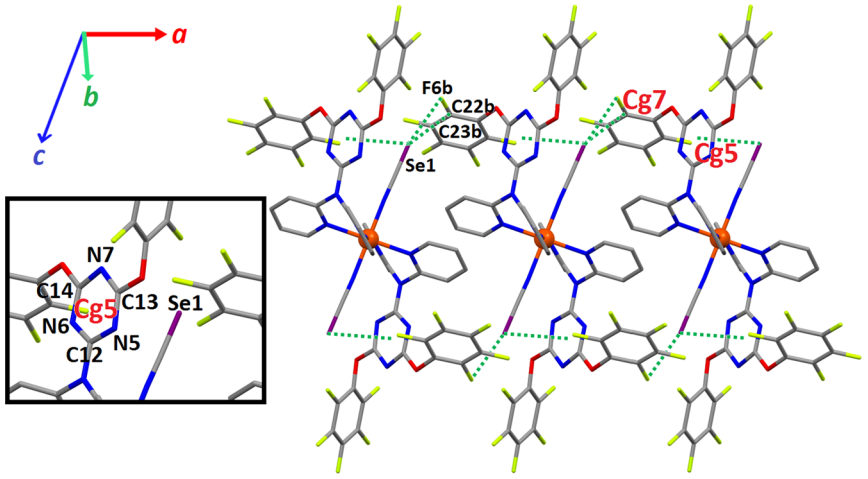

Figure 3. View of the crystal packing of LS $\mathbf{1}^{NCSe}$**·2PrCN** illustrating the occurrence of intermolecular lone pair$\cdots\pi$ interactions (green dotted lines) between the selenocyanate anions and adjacent pentafluorophenoxy moieties (Se1···C22b = 3.531(2) Å, Se1···C23b = 3.772(2) Å, and Se1···F6b = 3.192(1) Å) and intramolecular lone pair$\cdots\pi$ interactions between the selenocyanate anions and triazine rings (Se1···Cg5 = 3.585(1) Å). The inset shows the labeling of the atoms involved in lone pair$\cdots\pi$ interactions. Symmetry operation: $b = -1 + x, y, z$.

$N_{pyridine}$ and 1.948(3) Å for Fe−N_{NCSe} (Table 1), suggest the occurrence of a 1:7 HS/LS mixture, as estimated by properly weighing the bond length values found for the pure LS and HS states, shown in Table 1. In fact, the χT value of about 0.42 cm^3 mol^{-1} obtained at 260 K by bulk magnetic studies (see Magnetic and Thermal Studies section) indicates the presence of ca. 15% HS centers, in fair agreement with the structural results.

The octahedral distortion parameters Σ and Φ estimate the magnitude of the deformation of the coordination geometry with respect to a perfect octahedron (for which the Σ and Φ values are 0).[43−45] Upon LS → HS transition, the coordination angles vary from 86.25(6) and 93.75(6)° to 82.85(13) and 97.15(13)°, respectively; as the angles move away from the ideal value of 90°, the increased distortion of the octahedron can be interpreted by the entropy-driven SCO phenomenon.[46] Accordingly, for LS $\mathbf{1}^{NCSe}$, Σ = 31 and Φ = 25, and these values are increased for HS $\mathbf{1}^{NCSe}$ to 44 and 64, respectively (Table 1). The ΔΣ ($\Sigma_{HS} - \Sigma_{LS}$) and ΔΦ ($\Phi_{HS} - \Phi_{LS}$) parameters characterize the extent of the structural changes induced by the spin transition. For $\mathbf{1}^{NCSe}$, ΔΣ and ΔΦ amount to 13 and 39, respectively; the rather high ΔΦ value is indicative of an alteration of the octahedral geometry when the iron(II) centers transit from the LS to the HS state. Such strong structural

dx.doi.org/10.1021/ic501389s | *Inorg. Chem.* 2014, 53, 9827−9836

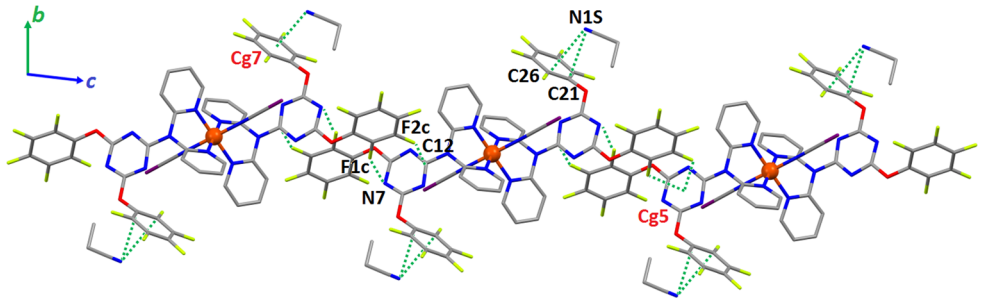

Figure 4. View of the crystal packing of LS $\mathbf{1}^{NCSe}$**·2PrCN** showing the formation of a supramolecular 1D chain along the crystallographic *c* axis through double lone pair(C_6F_5)···π(triazine) interactions characterized by the short contact distances N7···F1c = 3.104(2) Å and C12···F2c = 3.014(2) Å. Symmetry operation: $c = 2 - x, 1 - y, 2 - z$.

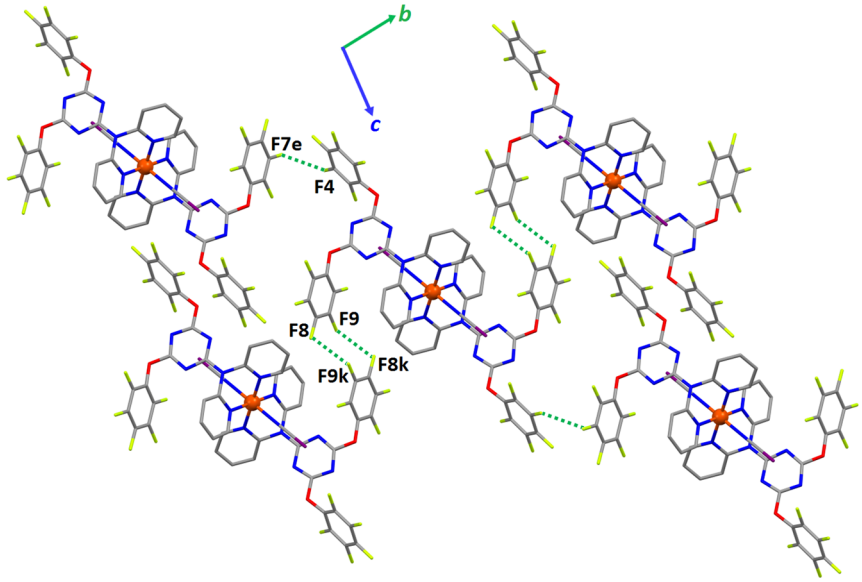

Figure 5. View of the crystal packing of LS $\mathbf{1}^{NCSe}$**·2PrCN** showing the formation of 2D sheets in the *bc* plane by means of strong F···F bonding contacts (green dotted lines; F8···F9k = 2.780(2) Å and F4···F7e = 2.885(2) Å). Symmetry operations: $e = 2 - x, 2 - y, 2 - z$; $k = 2 - x, 2 - y, 1 - z$.

deformation may affect the mutual interaction, in the crystal, of the transition metal ions spins, hence potentially enhancing the cooperativity between the switching sites that would lead to an abrupt LS ↔ HS crossover event.[43] Because the ΔΦ value of the related thiocyanate compound $\mathbf{1}^{NCS}$**·2MeCN** is also high (namely, 36[37]), cooperative behavior may be expected as well for solid $\mathbf{1}^{NCSe}$**·2PrCN**.

The crystal packing of LS $\mathbf{1}^{NCSe}$**·2PrCN** reveals an intricate network of supramolecular interactions that strongly connect the iron(II) molecules. The metal complexes form a 1D supramolecular chain along the crystallographic *c* axis by means of parallel-displaced π···π interactions involving pentafluorophenoxy rings (Figure 2A). Actually, a very strong lone pair···π contact[47,48] is observed between the oxygen atom O1 and a neighboring pentafluorophenoxy unit; for instance, the contact distance O1···C20g of 3.076(2) Å is significantly below the sum of the van der Waals radii of O and C (i.e., 3.22 Å). Moreover, the C15···C20g contact distance of 3.323(2) Å also reflects a strong arene···arene stacking interaction (the sum of the van der Waals radii of two C atoms is 3.40 Å). In fact, the C_6F_5O···C_6F_5O contacts are shorter in LS $\mathbf{1}^{NCSe}$**·2PrCN** compared to LS $\mathbf{1}^{NCS}$**·2MeCN** (for which the shortest O···C contact distance amounts to 3.112(2) Å[37]). Similar to that of $\mathbf{1}^{NCS}$**·2MeCN**, the iron(II) complexes are associated through nearly face-to-face π···π interactions between coordinated pyridine to generate another 1D chain that runs along the crystallographic *a* axis (Figure 2B). These supramolecular bonds are characterized by a centroid-to-centroid distance Cg4···Cg4p of 3.682(1) Å, which again is smaller than that of $\mathbf{1}^{NCS}$**·2MeCN** (3.757(1) Å[37]). Along the *a* direction, the 1D supramolecular chains are further stabilized via lone pair···π contacts involving the selenocyanate anions (Figure 3). Thus, the selenium atom Se1 interacts with an adjacent pentafluorophenoxy ring (Se1···Cg7 distance of 4.320(1) Å; Table 1), with the shortest contact distances being Se1···C22b = 3.531(2) Å and Se1···C23b = 3.772(2) Å (Figure 3), which are close to the sum of the van der Waals radii of Se and C, namely, 3.60 Å. In addition, a very short close contact is observed between Se1 and F6b; indeed, the corresponding separation value of 3.192(1) Å is well below the sum of the van der Waals radii of Se and F, i.e., 3.37 Å. Se1 is also involved in an intramolecular lone pair···π interaction with a triazine ring (Se1···Cg5 = 3.585(1) Å; Figure 3 and Table 1).

Along the *c* direction, the formation of another type of 1D chain is observed, which is formed through double lone pair (C_6F_5)···π(triazine) interactions (Figure 4), with centroid-to-fluorine distances Cg5···F1c and Cg5···F2c of 3.238(2) and 3.443(2) Å, respectively (Table 1). These 1D chains are

dx.doi.org/10.1021/ic501389s | *Inorg. Chem.* 2014, 53, 9827−9836

connected to the chains formed by the parallel-displaced $\pi_{C6F5O}\cdots\pi_{C6F5O}$ interactions (see above and Figure 2A), in a parallel fashion. Furthermore, the chains interact with the lattice propionitrile molecules via lone pair$\cdots\pi$ contacts with pentafluorophenoxy rings (Figure 4). These noncovalent bonding interactions are characterized by distances of N1S$\cdots$C21 = 3.202(3) Å and N1S$\cdots$C26 = 3.278(3) Å (Figure 4 and Table 1; N1S$\cdots$Cg7 = 3.413(2) Å), which are within the sum of the van der Waals radii of N and C, i.e., 3.25 Å.

The 2D supramolecular sheets in the *ac* plane are connected to each other by triple strong F$\cdots$F bonds (*bc* plane; Figure 5); indeed, the contact distances F8$\cdots$F9k and F8k$\cdots$F9 of 2.780(2) Å and F4$\cdots$F7e of 2.885(2) Å (Table 1) are all below the sum of the van der Waals radii of two F atoms, namely, 2.94 Å.[49] All of these supramolecular bonding interactions generate a 3D framework of tightly packed iron(II) complexes, indicating the likely cooperative character of the SCO, as indeed corroborated by magnetic and thermal studies (see below).

Furthermore, the magnetic and thermal studies disclose an interesting behavior of **1^{NCSe}·2PrCN** upon aging or annealing (see Magnetic and Thermal Studies section). Indeed, a displacement of the transition temperature toward a lower value is observed upon progressive loss of lattice propionitrile molecules. To understand this phenomenon, we have attempted several crystallographic studies on single crystals of **1^{NCSe}·2PrCN**. First, measurements at temperatures above 300 K typically resulted in rapid crystal degradation, impeding the determination of the structure. Actually, **1^{NCSe}·2PrCN** also degrades within a few days, when left in air, at room temperature.

Following the strategy adopted for the magnetic studies (see below), i.e., warming to 300 or 320 K for short periods of time and subsequent cooling to 100 K (see Scheme S1), we have collected seven single-crystal X-ray diffraction data sets of **1^{NCSe}·2PrCN** (see details in Table S1). No changes are observed around the iron(II) ion (see Table S2 for pertinent metric data) or in the crystal lattice, where the propionitrile molecules are found. However, as manifested by a slight worsening of the agreement indices, these temperature-dependent studies have led to a progressive deterioration of the single crystal. Further thermal annealing above 320 K results in the complete loss of crystallinity; accordingly, the structural modifications associated with the elimination of propionitrile molecules from the crystal lattice could not be assessed by single-crystal diffraction studies.

Magnetic and Thermal Studies. Differential scanning calorimetry measurements on freshly prepared polycrystalline powders showed an endothermic/exothermic event upon warming/cooling, as expected for the SCO transition occurring in **1^{NCSe}·2PrCN**. However, upon repeating the measurements on powders left in contact with air, a second anomaly appeared at lower temperatures, whereas the original one was significantly lowered. After 1 week in contact with air, only this second anomaly at lower temperatures remained (Figure S1). In a similar manner, variable-temperature magnetic measurements showed a behavior highly dependent on the thermal history of the sample within the magnetometer (see Figure S2 for a χT vs T plot, where χ is the molar paramagnetic susceptibility). The first heating scan, performed up to 350 K, evidenced a complete thermal SCO centered at ca. 283 K, whereas the first cooling (to 5 K) and second heating (to 330 K) scans showed a conversion occurring in two similar steps centered at ca. 280 and 215 K. After this second warming scan, the conversion occurred again as a single step centered at ca. 217 K. No further variation of the behavior was then detected in further temperature scans. The similarity between the observations made with these two techniques points to a modification of **1^{NCSe}·2PrCN** occurring upon prolonged air exposure at RT or shorter periods of time at temperatures in the 330−350 K range in a He depression (the sample is subjected to vacuum at room temperature prior to insertion in the magnetometer sample space, so the modification seems to require slightly higher temperatures than 300 K), in agreement with the rapid loss of crystallinity of single crystals observed above 320 K. The two-step magnetic transition (evidenced also by the two DSC anomalies) corresponds to a situation in which two distinct phases are present in the material, i.e., with partial modification of pristine **1^{NCSe}·2PrCN**. Thermogravimetric measurements were thus carried out to ascertain a possible loss of the lattice propionitrile molecules. The data shows a 6.6% weight loss centered at 382 K, with an onset at around 330 K (Figure S3). These data agree perfectly with the loss of all propionitrile molecules from the crystal lattice (theoretical value, 6.86%). Under the dynamic conditions used here, the loss of propionitrile is completed at ca. 390 K, slightly above its conventional boiling temperature at ambient pressure. Clearly, upon moderate heating, **1^{NCSe}·2PrCN** tends to lose its lattice propionitrile, which, in the solid state, is only weekly bound by van der Waals interactions. Powder diffraction methods reveal that the resulting material is polycrystalline, with an infrared spectrum almost identical to that of **1^{NCSe}·2PrCN**; notably, the $NCSe^-$ vibrations at 2055 and 2098 cm^{-1} slightly broaden, the former being shifted by ca. 6 cm^{-1} toward lower wavenumbers (Figure S4). Not unexpectedly, the modified phase can thus be ascribed to desolvated **1^{NCSe}**.

The temperature dependence of the χT product of **1^{NCSe}·2PrCN** and **1^{NCSe}**, obtained reproducibly by thermal annealing of fresh **1^{NCSe}·2PrCN** for 2 h at 80 °C, is depicted in Figure 6, evidencing LS ↔ HS transitions centered on 283 and 220 K for **1^{NCSe}·2PrCN** and **1^{NCSe}**, respectively. The conversions are complete, with χT increasing from ca. 0.02−0.04 $cm^3\ mol^{-1}\ K$

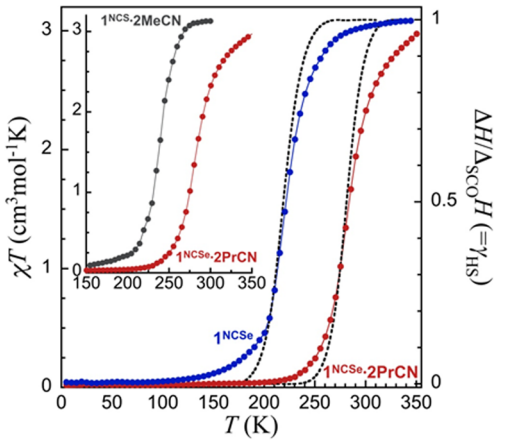

Figure 6. χT vs T plot for **1^{NCSe}·2PrCN** (red dots) and **1^{NCSe}** (blue dots) depicting their full SCO process and corresponding temperature dependence of their excess enthalpies normalized to that involved in the process of SCO (black dashed lines). Note that the latter is equivalent to the temperature dependence of the HS fraction $\gamma_{HS}(T)$. The inset χT vs T plot compares the SCO of **1^{NCSe}·2PrCN** with that of the analogue compound **1^{NCS}·2MeCN** (gray dots). Full lines are guides to the eye.

dx.doi.org/10.1021/ic501389s | *Inorg. Chem.* 2014, 53, 9827−9836

below 220 K and above 120 K, respectively, a typical value for an Fe(II) ion in a LS $S = 0$ state, to ca. 2.97 $cm^3\ mol^{-1}\ K$ at 350 K and ca. 3.04−3.08 $cm^3\ mol^{-1}\ K$ above 300 K, respectively; both values are indicative of a mostly HS $S = 2$ state.

The SCO curves of both materials are indeed very similar in shape, with that of $\mathbf{1}^{\mathbf{NCSe}}$ simply being shifted to lower temperatures by ca. 63 K. The value of ΔT_{80}, the temperature range over which 80% of the LS ↔ HS conversion takes place, is indeed the same at about 65 K, slightly higher than that observed for $\mathbf{1}^{\mathbf{NCS}}$**·2MeCN**, namely, $\Delta T_{80} \approx 50$ K (see inset of Figure 6).[37] This less efficient cooperative character shown by $\mathbf{1}^{\mathbf{NCSe}}$**·2PrCN** (compared to that of $\mathbf{1}^{\mathbf{NCS}}$**·2MeCN**) might be interpreted by two concurrent effects: the presence of bulkier propionitrile molecules, compared to acetonitrile, and that of the more diffuse Se atom, resulting in weaker supramolecular interactions (with respect to those involving an S atom) and molecules and Fe(II) ions being kept (on average) further apart than when S atoms are present. This latter contribution seems to be particularly relevant, as the desolvated $\mathbf{1}^{\mathbf{NCSe}}$ material has a similar (larger) ΔT_{80} (of ca. 70 K).

The temperature dependence of the molar heat capacity of $\mathbf{1}^{\mathbf{NCSe}}$**·2PrCN** and $\mathbf{1}^{\mathbf{NCSe}}$ exhibit a marked anomaly, in the 240−320 and 180−260 K ranges, respectively, and culminating at 280 and 218 K (Figure 7, top). These features are in perfect agreement with the magnetic data and are thus due to the SCO process in $\mathbf{1}^{\mathbf{NCSe}}$**·2PrCN** and $\mathbf{1}^{\mathbf{NCSe}}$. The corresponding excess heat capacities allow the associated excess enthalpy and entropy to be determined as 9.71 kJ mol^{-1} and 34.6 J $mol^{-1}\ K^{-1}$, respectively, for $\mathbf{1}^{\mathbf{NCSe}}$**·2PrCN** and 8.27 kJ mol^{-1} and 37.9 J $mol^{-1}\ K^{-1}$ for $\mathbf{1}^{\mathbf{NCSe}}$. Normalizing $\Delta H(T)$ to the corresponding ΔH_{SCO} also provides the temperature variation of the HS fraction, $\gamma_{HS}(T)$, depicted as dashed lines in Figure 6, which is again in excellent agreement with the magnetic data. To provide a comparable estimation of the cooperative character of the SCO in $\mathbf{1}^{\mathbf{NCSe}}$**·2PrCN** and $\mathbf{1}^{\mathbf{NCSe}}$, their excess heat capacities were fitted to Sorai's domain model (see the Supporting Information for details),[50] often used in SCO systems, cooperative or not, for which accurate calorimetric data are available.[51−54] The model gives a measure of the cooperativity through the number, n, of like-spin SCO centers per interacting domain. Here, the derived best fits (red lines in Figure 7, bottom) provide moderate numbers of interacting molecules per domain at $n = 8.1$ and 5.2 for $\mathbf{1}^{\mathbf{NCSe}}$**·2PrCN** and $\mathbf{1}^{\mathbf{NCSe}}$, respectively. These values are in the same range as that of the $\mathbf{1}^{\mathbf{NCS}}$**·2MeCN** analogue ($n = 6.2$) and indicate a similar cooperative character of the SCO in these materials, significantly inferior to the value of 14.2 we recently reported for the related $[Fe(\mathbf{L1})_2(NCS)_2]\cdot 2CH_3OH$ (**L1** = 2-chloro-4-(*N*,*N*-(2-pyridyl)amino)-6-(pentafluorophenoxy)-(1,3,5)-triazine).[42] Although it gives rise to a decrease in the SCO temperature by nearly 60 K, the loss of the lattice propionitrile molecule does not seem to affect significantly the way the electronic transition couples to the lattice phonons, the major component of the SCO cooperativeness.

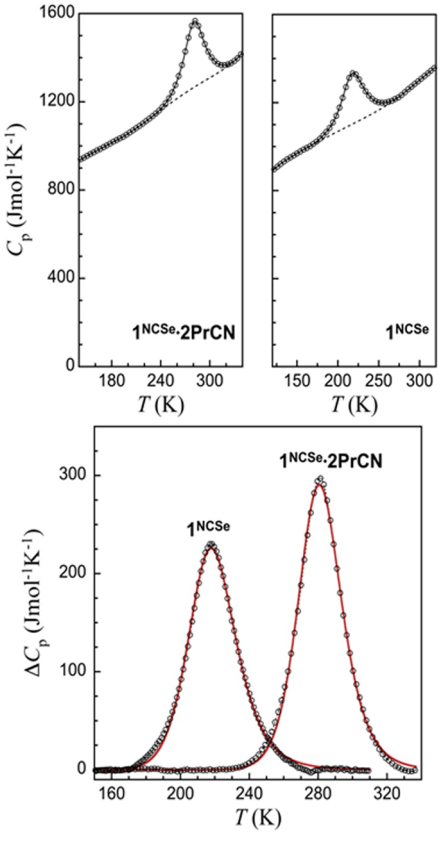

Figure 7. (Top) Molar heat capacities of $\mathbf{1}^{\mathbf{NCSe}}$**·2PrCN** and $\mathbf{1}^{\mathbf{NCSe}}$ showing a significant endothermic anomaly arising from the process of SCO. The dashed lines are the respective estimated lattice components. (Bottom) Excess molar heat capacities associated with the SCO of $\mathbf{1}^{\mathbf{NCSe}}$**·2PrCN** and $\mathbf{1}^{\mathbf{NCSe}}$. The full red lines are fits to Sorai's domain model (see text and ref 50), with $n = 8.1$ and $T_{SCO} = 281.7$ K and $n = 5.2$ and $T_{SCO} = 219.4$ K for $\mathbf{1}^{\mathbf{NCSe}}$**·2PrCN** and $\mathbf{1}^{\mathbf{NCSe}}$, respectively.

X-ray Powder Diffraction Studies. As mentioned above, the temperature effect on the solid-state structure of $\mathbf{1}^{\mathbf{NCSe}}$**·2PrCN** (with possible structural changes) could not be investigated by single-crystal X-ray diffraction as a result of the degradation of the material when $T > 320$ K. Therefore, X-ray powder-diffraction studies were carried out to explore potential temperature-dependent structural changes in $\mathbf{1}^{\mathbf{NCSe}}$**·2PrCN**. Powder diffraction data, collected in the 300−370 K range (shown in Figure 8) and analyzed by the structureless Le Bail whole pattern profile method, allowed the relative changes of the lattice parameters to be retrieved (cell volume and the size and shape of the thermal strain tensor). These results are numerically reported in Table 2 and are graphically depicted in Figure 9. The shape and orientation of the thermal strain tensor, elongated in the $[1\bar{1}0]$ direction, was then compared with the known crystal structure, which evidenced the presence of weakly bound slabs parallel to the $(1\bar{1}0)$ plane and is thus prone to more significant thermally induced dilatation.

Prolonged heating at 370 K showed a progressive change of the diffraction trace, which was completed after ca. 1 h. After eliminating a few peaks (attributed to an unknown contaminant), a reliable unit cell for the HT phase was obtained (using TOPAS-R):[55] $a = 8.87$, $b = 11.21$, $c = 15.40$ Å, $\alpha = 102.3$, $\beta = 84.3$, and $\gamma = 103.4°$, $V = 1454$ Å^3; GOF(20) = 21.[56] The crystal symmetry and the lattice parameters herein proposed match those found for the pristine solvated phase (see Table S1, $V = 1557$ Å^3 at 300 K). The difference in the molar volume ($\Delta V = -103$ Å^3) is well-matched with that expected for the loss of two PrCN molecules (64 Å^3, as estimated by SMILE[57]). After cooling to room temperature, diffraction data were collected with an overnight measurement (shown in Figure S5). Unfortunately, the powder pattern, due to partial degradation, contained too many peaks, making the crystal structure determination of the desolvated phase impossible.

dx.doi.org/10.1021/ic501389s | Inorg. Chem. 2014, 53, 9827−9836

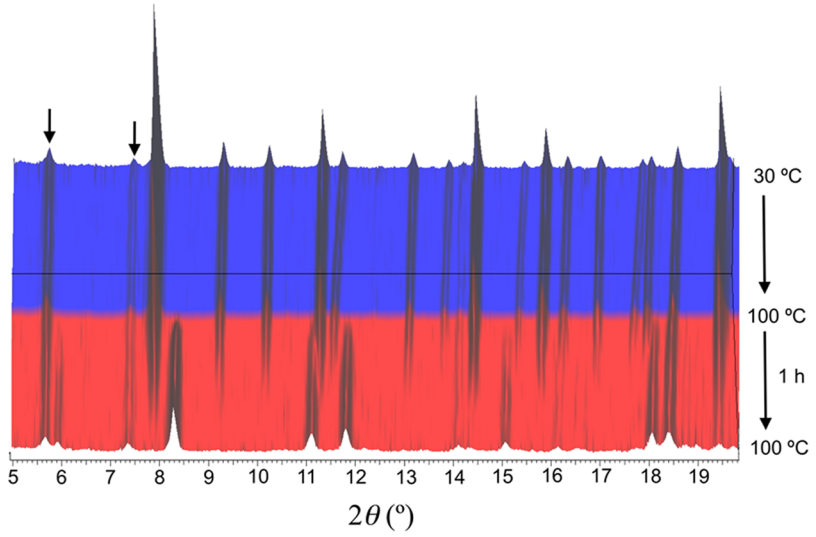

Figure 8. Variable-temperature X-ray powder diffraction data, collected between 30 and 100 °C. Vertical axis (back to front: temperature increase). The blue portion refers to the pristine **1**^{NCSe}**·2PrCN** species, transforming into the (still triclinic and contracted, see text) unsolvated phase (the two weak low-angle peaks at 5.6 and 7.3°, highlighted by the black arrows, belong to an unknown contaminant generated by partial degradation). The red portion contains 12 XRPD traces collected under isothermal conditions (in air) at 100 °C (5 min each).

Table 2. Linear and Volumetric Thermal Expansion Coefficients of 1^{NCSe}.2PrCN in the Form of $\partial \ln x/\partial T$ (x = a, b, c, α, β, γ and V)[a]

$\partial \ln a/\partial T$	$\partial \ln b/\partial T$	$\partial \ln c/\partial T$	$\partial \ln \alpha/\partial T$	$\partial \ln \beta/\partial T$	$\partial \ln \gamma/\partial T$	$\partial \ln V/\partial T$
+160	+74	+78	+9	−18	+78	+227

[a]Units in M K^{-1}. Values were computed by fitting the TXRPD-derived data in the 30−95°C range, where a nearly linear trend was observed.

The loss of the lattice propionitrile molecules will irremediably affect the solid-state packing of the iron(II) complexes. Actually, the propionitrile molecules connect the [Fe(**L1**^{F})$_2$(NCSe)$_2$] complexes, through lone pair···π interactions (Figure 10), generating a 1D supramolecular chain, and are therefore involved in the observed SCO properties of **1**^{NCSe}**·2PrCN**. Consequently, their removal will have an effect on the magnetic properties of the material (Figure S6). In fact, the spin-transition properties of the propionitrile-free compound **1**^{NCSe} are modified compared to those of **1**^{NCSe}**·2PrCN** (see above), as reflected by the lower $T_{1/2}$ (220 K instead of 283 K) and slightly lower cooperativity ($n/\Delta T_{80}$ value of ca. 5.2/70 K instead of 8.1/65 K).

EXPERIMENTAL SECTION

Physical Measurements. Infrared spectra were recorded with a Nicolet 5700 FT-IR spectrometer (as KBr pellets) or with a PerkinElmer Spectrum 100 apparatus equipped with an ATR device (neat samples). ^{1}H NMR spectra were recorded at room temperature with a Varian Unity 300 MHz spectrometer; chemical shifts are reported in ppm relative to the residual solvent signal of $CDCl_3$ (δ = 7.26 ppm). Elemental analyses were performed by the Servei de Microanalisi, Consejo Superior de Investigaciones Científicas (CSIC) of Barcelona. Thermogravimetric measurements were performed with a SDT2960 thermobalance from TA Instruments under synthetic air at 10 °C min^{-1}.

Magnetic measurements were performed on bulk microcrystalline powders using a commercial SQUID magnetometer of the Physical Measurements unit of the Servicio General de Apoyo a la Investigación−SAI, Universidad de Zaragoza. Correction for the experimentally measured contribution of the sample holder and the sample diamagnetism, estimated from Pascal's tables, were applied. In this setup, the sample space is maintained under a low-pressure He atmosphere, with the sample being held within a gelatin capsule and thus subjected to dry depression.

Differential scanning calorimetry (DSC) experiments were performed with a Q1000 calorimeter from TA Instruments equipped with the LNCS accessory. The temperature and enthalpy scales were calibrated with a standard sample of indium, using its melting transition (156.6 °C, 3296 J mol^{-1}). The measurements were carried out using aluminum pans with a mechanical crimp, with an empty pan as reference. The zero-heat flow procedure described by TA Instruments was followed to derive heat capacities, using synthetic sapphire as reference compound. An overall accuracy of ca. 0.2 K for the temperature and up to 5−10% for the heat capacity was estimated over the whole temperature range by comparison with the synthetic sapphire. A lattice heat capacity was estimated from data below and above the anomaly associated with the SCO process (dashed lines in Figure 7, top). Excess enthalpy and entropy were derived by integration of the excess heat capacity with respect to T and ln T, respectively.

Materials. The ligand 2-(*N*,*N*-bis(2-pyridyl)amino)-4,6-bis-(pentafluorophenoxy)-(1,3,5)triazine (**L1**^{F}) was prepared according to the literature.[37] $Fe(ClO_4)_2{\cdot}6H_2O$, ascorbic acid, KNCSe, and propionitrile were purchased from Sigma-Aldrich and used as supplied.

Synthesis of [Fe(L1^F)$_2$(NCSe)$_2$]·2CH$_3$CH$_2$CN (1^{NCSe}·2PrCN). A solution of ligand **L1**^{F} (0.122 g, 0.20 mmol) in propionitrile (5 mL) was added to a solution of $Fe(ClO_4)_2{\cdot}6H_2O$ (0.026 g, 0.10 mmol) in propionitrile (2 mL) containing ca. 5 mg of ascorbic acid (to prevent oxidation to iron(III)). Next, a solution of KNCSe (0.029 g, 0.20 mmol) in propionitrile (3 mL) was added, and the resulting light-yellow reaction mixture was filtered. The filtrate was left unperturbed for the slow evaporation of the solvent; after 4 days, single crystals of **1**^{NCSe}**·2PrCN**, suitable for X-ray diffraction analysis, were obtained with a yield of 60% (0.096 g, 0.06 mmol, based on iron). Elemental analyses calculated (found) (%) for $C_{58}H_{26}F_{20}FeN_{16}O_4Se_2$: C, 43.41 (43.59); H, 1.63 (1.67); N, 13.97 (13.81). IR (KBr): ν = 2096(w), 2061(m), 1607(m), 1558(m), 1521(s), 1471(m), 1437(w), 1371(s),

dx.doi.org/10.1021/ic501389s | Inorg. Chem. 2014, 53, 9827−9836

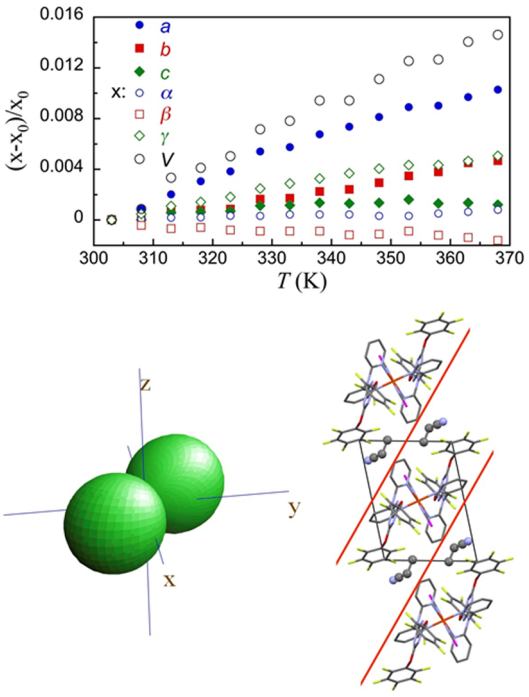

Figure 9. (Top) Relative lattice parameter changes (including cell volume), measured by TXRPD data. Horizontal axis, temperature (T, K); vertical axis, $(x_T - x_{30})/x_{30}$ (x = a, b, c, α, β, γ, and V). (Bottom left) Thermal strain tensor for the 30−95 °C range, computed by Ohashi's method[63] and drawn with Wintensor.[64] (Bottom right) Crystal packing of **1**^{NCSe}**·2PrCN** viewed approximately down [110], highlighting the $(1\bar{1}0)$ plane, separating slabs of weakly bound molecules, which conform to the longest axis of the thermal strain tensor shown on the left.

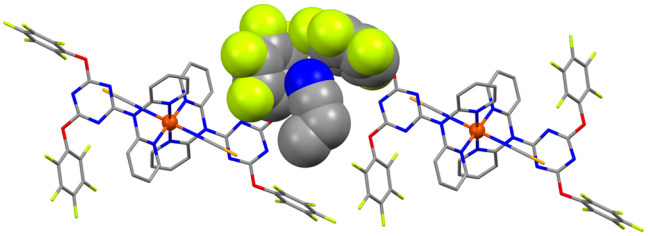

Figure 10. View of the solid-state structure of **1**^{NCSe}**·2PrCN** showing the interaction of a propionitrile molecule with two pentafluorophenyl rings (in space-filling mode) belonging to two neighboring iron(II) complexes, through lone pair···π interactions.

1307(m), 1244(m), 1158(m), 1079(m), 1001(m), 978(m), 806(w), 778(w), 644(w) cm^{-1}.

Single-Crystal X-ray Crystallography. X-ray diffraction data for **1**^{NCSe}**·2PrCN** were collected on a yellow (purple at 100 K) needle with a Bruker APEX II CCD diffractometer on the Advanced Light Source beamline 11.3.1 at Lawrence Berkeley National Laboratory from a silicon 111 monochromator (λ = 0.7749 Å). Seven data sets were acquired successively on the same crystal following the temperature sequence depicted in Scheme S1. Attempts at measuring at temperatures above 300 K or bringing crystals above 320 K for a longer period of time systematically resulted in loss of crystallinity. Data reduction and absorption corrections were performed with SAINT and SADABS, respectively.[58] The structures were solved using SIR97[59,60] and refined over F^2 using the SHELXTL suite.[58,61] Crystallographic and refinement parameters are summarized in Table S1. Selected bond distances and angles are given in Tables 1 and S2. All details can be found in the supplementary crystallographic data for this article in cif format with CCDC numbers 1007424−1007430. These data can be obtained free of charge from The Cambridge Crystallographic Data Centre via www.ccdc.cam.ac.uk/data_request/cif.

X-ray Powder Diffraction. Gently ground powders of **1**^{NCSe}**·2PrCN** were deposited in the hollow of a zero-background plate, 0.2 mm deep (a silicon monocrystal supplied by Assing SrL, Monterotondo, Italy). Diffraction experiments were performed on a vertical-scan Bruker AXS D8 Advance diffractometer in 2θ mode, equipped with a linear position-sensitive Lynxeye detector, primary beam Soller slits, and Ni-filtered Cu Kα radiation (λ = 1.5418 Å). Generator settings: 40 kV, 40 mA.

Thermodiffractometric (TXRPD) experiments were performed on a powdered batch of **1**^{NCSe}**·2PrCN**, deposited in the hollow of an aluminum-framed silicon monocrystal, mounted on a Peltier-driven sample heating stage, assembled by Officina Elettrotecnica di Tenno, Ponte Arche, Italy; diffractograms were acquired in air from 30 to 100 °C, with steps of 10 °C, in a significant low-angle 2θ range (5−20°) and, under isothermal conditions, at 100 °C for ca. 1 h. Lattice parameters at each T, for each phase, were refined by the structureless Le Bail procedure,[62] and linear thermal expansion coefficients were derived from data collected in the 30−100 °C range. Thermal strain tensors were computed using the STRAIN module available on the Bilbao Crystallographic Server following Ohashi's method.[63]

CONCLUSIONS

For about 8 years, our group and that of Murray[31] have been investigating the SCO properties of a particular family of iron(II) systems obtained from 2,2′-dipyridylamino-substituted triazine ligands. Through ligand design, it has been possible to obtain members of this group of SCO complexes with interesting properties.[42] In the present study, a new compound belonging to this family was prepared that exhibits solvent-dependent SCO properties. Indeed, the loss of propionitrile molecules present in the crystal lattice of **1**^{NCSe}**·2PrCN** results in a strong alteration of its SCO behavior, which is reflected by an important shift of the transition temperature, from $T_{1/2}$ = 283 K to 220 K (for the desolvated compound **1**^{NCSe}). This variation of the magnetic properties is most likely due to a modification of the crystal packing of the transiting molecules, hence exemplifying the great sensitivity of the SCO phenomenon. In addition, the results reported herein illustrate the potential of (2,2′-dipyridylamine/triazine)-based iron(II) complexes to generate SCO materials with singular properties.

ASSOCIATED CONTENT

Supporting Information

Crystallographic data for **1**^{NCSe}**·2PrCN** at different temperatures with the corresponding coordination bond distances and angles, DSC traces for fresh and aged **1**^{NCSe}**·2PrCN**, χT vs T plots, TGA of fresh **1**^{NCSe}**·2PrCN**, IR spectra of **1**^{NCSe}**·2PrCN** and **1**^{NCSe}, XRPD data for **1**^{NCSe}, and crystal packing views of **1**^{NCSe}**·2PrCN** showing the location of the lattice solvent molecules. This material is available free of charge via the Internet at http://pubs.acs.org.

AUTHOR INFORMATION

Corresponding Authors

*(N.M.) E-mail: norberto.masciocchi@uninsubria.it.
*(O.R.) E-mail: roubeau@unizar.es.
*(P.G.) E-mail: patrick.gamez@qi.ub.es.

Present Address

○Department of Chemistry, Faculty of Science and Technology, Thammasat University, Rangsit Campus, Klong 1, Klong Luang, Pathumthani 12121, Thailand.

Notes

The authors declare no competing financial interest.

■ ACKNOWLEDGMENTS

P.G. acknowledges ICREA (Institució Catalana de Recerca i Estudis Avançats) and the Ministerio de Economía y Competitividad of Spain (project CTQ2011-27929-C02-01). N.W. thanks the Royal Golden Jubilee Ph.D. Program (RGJ, grant no. PHD/0234/2550) and Khon Kaen University for a research grant. S.Y. acknowledges The Thailand Research Fund, the National Research University Project of Thailand, Office of the Higher Education Commission, through the Advanced Functional Materials Cluster of Khon Kaen University and the Center of Excellence for Innovation in Chemistry (PERCH-CIC), Office of the Higher Education Commission, Ministry of Education. The Advanced Light Source is supported by the Director, Office of Science, Office of Basic Energy Sciences of the U.S. Department of Energy under contract no. DE-AC02-05CH11231. O.R. acknowledges funding from the Ministerio de Economía y Competitividad of Spain (project MAT2011-24284).

■ REFERENCES

(1) Gütlich, P.; Goodwin, H. A. *Top. Curr. Chem.* **2004**, *233*, 1−47.
(2) *Spin-Crossover Materials: Properties and Applications*; Halcrow, M. A., Ed.; John Wiley and Sons: Chichester, UK, 2013.
(3) Boča, R. *A Handbook of Magnetochemical Formulae*; Elsevier: London, 2012; pp 159−186.
(4) Real, J. A.; Gaspar, A. B.; Munoz, M. C. *Dalton Trans.* **2005**, 2062−2079.
(5) Bousseksou, A.; Molnár, G.; Real, J. A.; Tanaka, K. *Coord. Chem. Rev.* **2007**, *251*, 1822−1833.
(6) Gütlich, P.; Hauser, A.; Spiering, H. *Angew. Chem., Int. Ed. Engl.* **1994**, *33*, 2024−2054.
(7) Cambi, L.; Szego, L. *Ber. Dtsch. Chem. Ges.* **1931**, *64*, 2591−2598.
(8) Cluster Issue: Spin-Crossover Complexes *Eur. J. Inorg. Chem.* **2013**, 573−1070.
(9) Krober, J.; Codjovi, E.; Kahn, O.; Grolière, F.; Jay, C. *J. Am. Chem. Soc.* **1993**, *115*, 9810−9811.
(10) Cantin, C.; Daubric, H.; Kliava, J.; Servant, Y.; Sommier, L.; Kahn, O. *J. Phys.: Condens. Matter* **1998**, *10*, 7057−7064.
(11) Kahn, O.; Martinez, C. J. *Science* **1998**, *279*, 44−48.
(12) Roubeau, O. *Chem.—Eur. J.* **2012**, *18*, 15230−15244.
(13) Létard, J. F.; Guionneau, P.; Goux-Capes, L. *Top. Curr. Chem.* **2004**, *235*, 221−249.
(14) Gaspar, A. B.; Seredyuk, M.; Gütlich, P. *Coord. Chem. Rev.* **2009**, *253*, 2399−2413.
(15) Gamez, P.; Costa, J. S.; Quesada, M.; Aromí, G. *Dalton Trans.* **2009**, 7845−7853.
(16) Bousseksou, A.; Molnár, G.; Salmon, L.; Nicolazzi, W. *Chem. Soc. Rev.* **2011**, *40*, 3313−3335.
(17) Gütlich, P.; Garcia, Y.; Goodwin, H. A. *Chem. Soc. Rev.* **2000**, *29*, 419−427.
(18) Sato, O. *Proc. Jpn. Acad., Ser. B* **2012**, *88*, 213−225.
(19) Ruben, M.; Breuning, E.; Lehn, J. M.; Ksenofontov, V.; Renz, F.; Gütlich, P.; Vaughan, G. B. M. *Chem.—Eur. J.* **2003**, *9*, 4422−4429.
(20) Aromí, G.; Barrios, L. A.; Roubeau, O.; Gamez, P. *Coord. Chem. Rev.* **2011**, *255*, 485−546.
(21) Olguin, J.; Brooker, S. *Coord. Chem. Rev.* **2011**, *255*, 203−240.
(22) Boča, M.; Jameson, R. F.; Linert, W. *Coord. Chem. Rev.* **2011**, *255*, 290−317.
(23) Murray, K. S. *Eur. J. Inorg. Chem.* **2008**, 3101−3121.
(24) Halcrow, M. A. *Coord. Chem. Rev.* **2009**, *253*, 2493−2514.
(25) Kitchen, J. A.; Brooker, S. *Coord. Chem. Rev.* **2008**, *252*, 2072−2092.
(26) Quesada, M.; de la Peña-O'Shea, V. A.; Aromí, G.; Geremia, S.; Massera, C.; Roubeau, O.; Gamez, P.; Reedijk, J. *Adv. Mater.* **2007**, *19*, 1397−1402.
(27) Gamez, P.; de Hoog, P.; Lutz, M.; Driessen, W. L.; Spek, A. L.; Reedijk, J. *Polyhedron* **2003**, *22*, 205−210.
(28) Gamez, P.; de Hoog, P.; Lutz, M.; Spek, A. L.; Reedijk, J. *Inorg. Chim. Acta* **2003**, *351*, 319−325.
(29) Quesada, M.; Monrabal, M.; Aromí, G.; de la Peña-O'Shea, V. A.; Gich, M.; Molins, E.; Roubeau, O.; Teat, S. J.; MacLean, E. J.; Gamez, P.; Reedijk, J. *J. Mater. Chem.* **2006**, *16*, 2669−2676.
(30) Quesada, M.; de Hoog, P.; Gamez, P.; Roubeau, O.; Aromí, G.; Donnadieu, B.; Massera, C.; Lutz, M.; Spek, A. L.; Reedijk, J. *Eur. J. Inorg. Chem.* **2006**, 1353−1361.
(31) Scott, H. S.; Ross, T. M.; Chilton, N. F.; Gass, I. A.; Moubaraki, B.; Chastanet, G.; Paradis, N.; Létard, J. F.; Vignesh, K. R.; Rajaraman, G.; Battena, S. R.; Murray, K. S. *Dalton Trans.* **2013**, *42*, 16494−16509.
(32) Scott, H. S.; Ross, T. M.; Batten, S. R.; Gass, I. A.; Moubaraki, B.; Neville, S. M.; Murray, K. S. *Aust. J. Chem.* **2012**, *65*, 874−882.
(33) Ross, T. M.; Moubaraki, B.; Batten, S. R.; Murray, K. S. *Dalton Trans.* **2012**, *41*, 2571−2581.
(34) Ross, T. M.; Moubaraki, B.; Neville, S. M.; Batten, S. R.; Murray, K. S. *Dalton Trans.* **2012**, *41*, 1512−1523.
(35) Ross, T. M.; Moubaraki, B.; Turner, D. R.; Halder, G. J.; Chastanet, G.; Neville, S. M.; Cashion, J. D.; Létard, J. F.; Batten, S. R.; Murray, K. S. *Eur. J. Inorg. Chem.* **2011**, 1395−1417.
(36) Neville, S. M.; Leita, B. A.; Offermann, D. A.; Duriska, M. B.; Moubaraki, B.; Chapman, K. W.; Halder, G. J.; Murray, K. S. *Eur. J. Inorg. Chem.* **2007**, 1073−1085.
(37) Wannarit, N.; Roubeau, O.; Youngme, S.; Teat, S. J.; Gamez, P. *Dalton Trans.* **2013**, *42*, 7120−7130.
(38) Gomez, V.; Benet-Buchholz, J.; Martin, E.; Galán-Mascarós, J. R. *Chem.—Eur. J.* **2014**, *20*, 5369−5379.
(39) Costa, J. S.; Rodriguez-Jimenez, S.; Craig, G. A.; Barth, B.; Beavers, C. M.; Teat, S. J.; Aromí, G. *J. Am. Chem. Soc.* **2014**, *136*, 3869−3874.
(40) Wei, R. J.; Tao, J.; Huang, R. B.; Zheng, L. S. *Inorg. Chem.* **2011**, *50*, 8553−8564.
(41) Amoore, J. L. M.; Kepert, C. J.; Cashion, J. D.; Moubaraki, B.; Neville, S. M.; Murray, K. S. *Chem.—Eur. J.* **2006**, *12*, 8220−8227.
(42) Nassirinia, N.; Amani, S.; Teat, S. J.; Roubeau, O.; Gamez, P. *Chem. Commun.* **2014**, *50*, 1003−1005.
(43) Halcrow, M. A. *Chem. Soc. Rev.* **2011**, *40*, 4119−4142.
(44) Marchivie, M.; Guionneau, P.; Létard, J. F.; Chasseau, D. *Acta Crystallogr., Sect. B: Struct. Sci.* **2005**, *61*, 25−28.
(45) McCusker, J. K.; Rheingold, A. L.; Hendrickson, D. N. *Inorg. Chem.* **1996**, *35*, 2100−2112.
(46) König, E. *Struct. Bonding (Berlin, Ger.)* **1991**, *76*, 51−152.
(47) Mooibroek, T. J.; Gamez, P. *CrystEngComm* **2012**, *14*, 1027−1030.
(48) Mooibroek, T. J.; Gamez, P. *CrystEngComm* **2012**, *14*, 3902−3906.
(49) Mooibroek, T. J.; Gamez, P. *CrystEngComm* **2013**, *15*, 1802−1805.
(50) Sorai, M.; Nakazawa, Y.; Nakano, M.; Miyazaki, Y. *Chem. Rev.* **2013**, *113*, PR41−122.
(51) Nakamoto, T.; Tan, Z. C.; Sorai, M. *Inorg. Chem.* **2001**, *40*, 3805−3809.
(52) Roubeau, O.; deVos, M.; Stassen, A. F.; Burriel, R.; Haasnoot, J. G.; Reedijk, J. *J. Phys. Chem. Solids* **2003**, *64*, 1003−1013.
(53) Arcis-Castillo, Z.; Zheng, S.; Siegler, M. A.; Roubeau, O.; Bedoui, S.; Bonnet, S. *Chem.—Eur. J.* **2011**, *17*, 14826−14836.
(54) Roubeau, O.; Castro, M.; Burriel, R.; Haasnoot, J. G.; Reedijk, J. *J. Phys. Chem. B* **2011**, *115*, 3003−3012.
(55) *TOPAS*, 3.0; Bruker AXS: Karlsruhe, Germany, 2005.
(56) de Wolff, P. M. *J. Appl. Crystallogr.* **1968**, *1*, 108−113.
(57) Eufri, D.; Sironi, A. *J. Mol. Graphics* **1989**, *7*, 165−169.
(58) *SAINT, SADABS, and SHELXTL*; Bruker AXS Inc.: Madison, WI.

(59) Altomare, A.; Burla, M. C.; Camalli, M.; Cascarano, G. L.; Giacovazzo, C.; Guagliardi, A.; Moliterni, A. G. G.; Polidori, G.; Spagna, R. *J. Appl. Crystallogr.* **1999**, *32*, 115−119.
(60) Burla, M. C.; Camalli, M.; Carrozzini, B.; Cascarano, G. L.; Giacovazzo, C.; Polidori, G.; Spagna, R. *Acta Crystallogr., Sect. A* **1999**, *55*, 991−999.
(61) Sheldrick, G. M. *Acta Crystallogr., Sect. A* **2008**, *64*, 112−122.
(62) Le Bail, A.; Duroy, H.; Fourquet, J. L. *Mater. Res. Bull.* **1988**, *23*, 447−452.
(63) Ohashi, Y. In *Comparative Crystal Chemistry*; Hazen, R. M., Finger, L. W., Eds.; Wiley: New York, 1982; pp 92−102.
(64) Kaminsli, W. *WINTENSOR*, V.1.4; University of Washington: Seattle, WA, 2011.
(65) Guionneau, P.; Marchivie, M.; Bravic, G.; Létard, J. F.; Chasseau, D. *Top. Curr. Chem.* **2004**, *234*, 97−128.
(66) Quesada, M.; Prins, F.; Bill, E.; Kooijman, H.; Gamez, P.; Roubeau, O.; Spek, A. L.; Haasnoot, J. G.; Reedijk, J. *Chem.—Eur. J.* **2008**, *14*, 8486−8499.